AMERICAN SOCIETY FOR MICROBIOLOGY | Antimicrobial Agents and Chemotherapy®

ANTIVIRAL AGENTS

Mechanisms of Vesicular Stomatitis Virus Inactivation by Protoporphyrin IX, Zinc-Protoporphyrin IX, and Mesoporphyrin IX

Christine Cruz-Oliveira,[a] Andreza F. Almeida,[a] João M. Freire,[b]* Marjolly B. Caruso,[a] Maria A. Morando,[c,d] Vivian N. S. Ferreira,[a] Iranaia Assunção-Miranda,[e] Andre M. O. Gomes,[a] Miguel A. R. B. Castanho,[b] Andrea T. Da Poian[a]

Instituto de Bioquímica Médica Leopoldo de Meis, Universidade Federal do Rio de Janeiro, Rio de Janeiro, Brazil[a]; Instituto de Medicina Molecular, Faculdade de Medicina, Universidade de Lisboa, Lisbon, Portugal[b]; Centro Nacional de Ressonância Magnética Nuclear, Universidade Federal do Rio de Janeiro, Rio de Janeiro, Brazil[c]; Centro de Desenvolvimento Tecnológico em Saúde, Fiocruz, Rio de Janeiro, Brazil[d]; Instituto de Microbiologia Paulo Góes, Universidade Federal do Rio de Janeiro, Rio de Janeiro, Brazil[e]

ABSTRACT Virus resistance to antiviral therapies is an increasing concern that makes the development of broad-spectrum antiviral drugs urgent. Targeting of the viral envelope, a component shared by a large number of viruses, emerges as a promising strategy to overcome this problem. Natural and synthetic porphyrins are good candidates for antiviral development due to their relative hydrophobicity and pro-oxidant character. In the present work, we characterized the antiviral activities of protoprophyrin IX (PPIX), Zn-protoporphyrin IX (ZnPPIX), and mesoporphyrin IX (MPIX) against vesicular stomatitis virus (VSV) and evaluated the mechanisms involved in this activity. Treatment of VSV with PPIX, ZnPPIX, and MPIX promoted dose-dependent virus inactivation, which was potentiated by porphyrin photoactivation. All three porphyrins inserted into lipid vesicles and disturbed the viral membrane organization. In addition, the porphyrins also affected viral proteins, inducing VSV glycoprotein cross-linking, which was enhanced by porphyrin photoactivation. Virus incubation with sodium azide and α-tocopherol partially protected VSV from inactivation by porphyrins, suggesting that singlet oxygen ($^1O_2$) was the main reactive oxygen species produced by photoactivation of these molecules. Furthermore, $^1O_2$ was detected by 9,10-dimethylanthracene oxidation in photoactivated porphyrin samples, reinforcing this hypothesis. These results reveal the potential therapeutic application of PPIX, ZnPPIX, and MPIX as good models for broad antiviral drug design.

KEYWORDS photoactivation, porphyrin, singlet oxygen, vesicular stomatitis virus, viral inactivation

Received 10 January 2017 **Returned for modification** 20 January 2017 **Accepted** 21 March 2017

Accepted manuscript posted online 27 March 2017

Citation Cruz-Oliveira C, Almeida AF, Freire JM, Caruso MB, Morando MA, Ferreira VNS, Assunção-Miranda I, Gomes AMO, Castanho MARB, Da Poian AT. 2017. Mechanisms of vesicular stomatitis virus inactivation by protoporphyrin IX, zinc-protoporphyrin IX, and mesoporphyrin IX. Antimicrob Agents Chemother 61:e00053-17. https://doi.org/10.1128/AAC.00053-17.

Address correspondence to Christine Cruz-Oliveira, ccruz@bioqmed.ufrj.br, or Andrea T. Da Poian, dapoian@bioqmed.ufrj.br.

* Present address: João M. Freire, Institut Pasteur, Unité de Virologie Structurale, Département de Virologie, Paris, France.

C.C.-O. and A.F.A. contributed equally to this article.

Despite the increasing number of antiviral drugs available nowadays, therapeutics for viral diseases often fail due to drug resistance development by the target viruses. In the search for antiviral agents with a broad spectrum of activity against viruses, antiviral agents targeting the viral envelope, a component shared by a large number of viruses, emerge as promising compounds able to overcome the drug resistance problem. Porphyrins, amphipathic molecules able to interact with membranes, appear to be good candidates for the development of such antivirals. Porphyrins are formed by four pyrrole rings linked by methine bonds. The nitrogen atoms in the center of the ring form a pocket able to coordinate metallic ions, conferring to porphyrin the ability to absorb light at additional wavelengths and act in catalytic transformations (1). These activities allow porphyrins to be involved in important biological processes, such as respiration (heme) and photosynthesis (chlorophyll and bacteriochlorophyll) (2).

Many viruses of different families have been inactivated by porphyrins or porphyrin derivatives, including enveloped viruses, such as HIV-1 (3, 4), poxvirus (5), hepatitis B virus (6, 7), hepatitis C virus (7, 8), Marburg, Tacaribe, and Junin viruses (7), bovine herpesvirus (9), and dengue and yellow fever viruses (7, 10), as well as nonenveloped viruses, such as poliovirus (9). Porphyrins and their derivatives were also used as enhancers of the effects of other antiviral drugs, as was observed for the combination of heme (or its analogues) with zidovudine for the treatment of HIV-1 infection (11, 12), and some porphyrins were conjugated with the neuraminidase inhibitor zanamivir for the treatment of influenza virus infections (13).

The mechanism by which porphyrins act as antivirals is related to their hydrophobic and pro-oxidant characteristics. Due to their relative hydrophobicity, porphyrins are able to interact with biological membranes (14), so enveloped viruses are potential candidates for targeting by porphyrin and subsequent inactivation through viral envelope destabilization and oxidation. These molecules also induce the generation of reactive oxygen species (ROS), promoting lipid, protein, and nucleic acid oxidation (15–19). The properties of porphyrins vary according to their structure and the metal ion present in the center of the tetrapyrrole, as well as substituents attached to the pyrrolic rings or to the methine bridges (1). Additionally, porphyrins are colored compounds that undergo photoactivation, being widely used in photodynamic therapy (PDT), a method used for microorganism inactivation (2, 20, 21). Hepatitis A virus and HIV are examples of viruses efficiently inactivated by the use of porphyrins as photosensitizers in PDT (22, 23). Also, several enveloped viruses belonging to different families were strongly inactivated by phthalocyanines, molecules closely related to porphyrins (10, 24–28). The ability of porphyrins to act as photosensitizers is related to their property of catalyzing ROS generation. ROS generation by photosensitizers occurs through two different pathways that may occur separately or simultaneously (2, 20, 29). In the type I pathway, the superoxide anion or hydroxyl radical is generated through electron transfer from the excited photosensitizer, while the type II pathway involves singlet oxygen ($^1O_2$) generation by energy transfer from the photoactivated molecule (2, 20, 29).

In this work, we evaluated the antiviral activities and the mechanisms of action of three porphyrins, protoporphyrin IX (PPIX), zinc protoporphyrin IX (ZnPPIX), and mesoporphyrin IX (MPIX) (Fig. 1A, E, and I, respectively), using as a model an enveloped virus, vesicular stomatitis virus (VSV). VSV is a member of the *Rhabdoviridae* family and causes an acute disease that mainly affects cattle, pigs, and horses (30). The disease is characterized by the development of vesicles and ulcers in the oral cavity and, less frequently, in the teats and coronary bands, leading to decreases in milk and meat production. The VSV structure is composed of a nucleocapsid surrounded by the viral envelope. The envelope is a lipid bilayer derived from the host cell and contains trimers of a single type of an integral glycoprotein, named the G protein, which mediates virus entry into the target cell through endocytosis and catalyzes the fusion of viral and endosomal membranes, an essential step of infection (31). The nucleocapsid consists of the viral RNA genome tightly associated with the nucleoprotein (N). VSV RNA is a negative-sense, single-stranded molecule that depends on viral RNA-dependent RNA polymerase, a complex formed by the L protein and the phosphoprotein (P), to replicate (32). The virion also contains the matrix (M) protein, located between the envelope inner surface and nucleocapsid (33). We demonstrate that PPIX, ZnPPIX, and MPIX inactivate VSV and that their antiviral activities are strongly enhanced by porphyrin photoactivation. We found that, besides the interaction of the porphyrins with the viral envelope, which is destabilized, these molecules promote viral protein cross-linking and degradation. The use of antioxidants and spectroscopic analyses revealed that $^1O_2$ is the main reactive species produced by the photoactivated porphyrin, with the type II pathway being the mechanism of porphyrin-induced VSV inactivation.

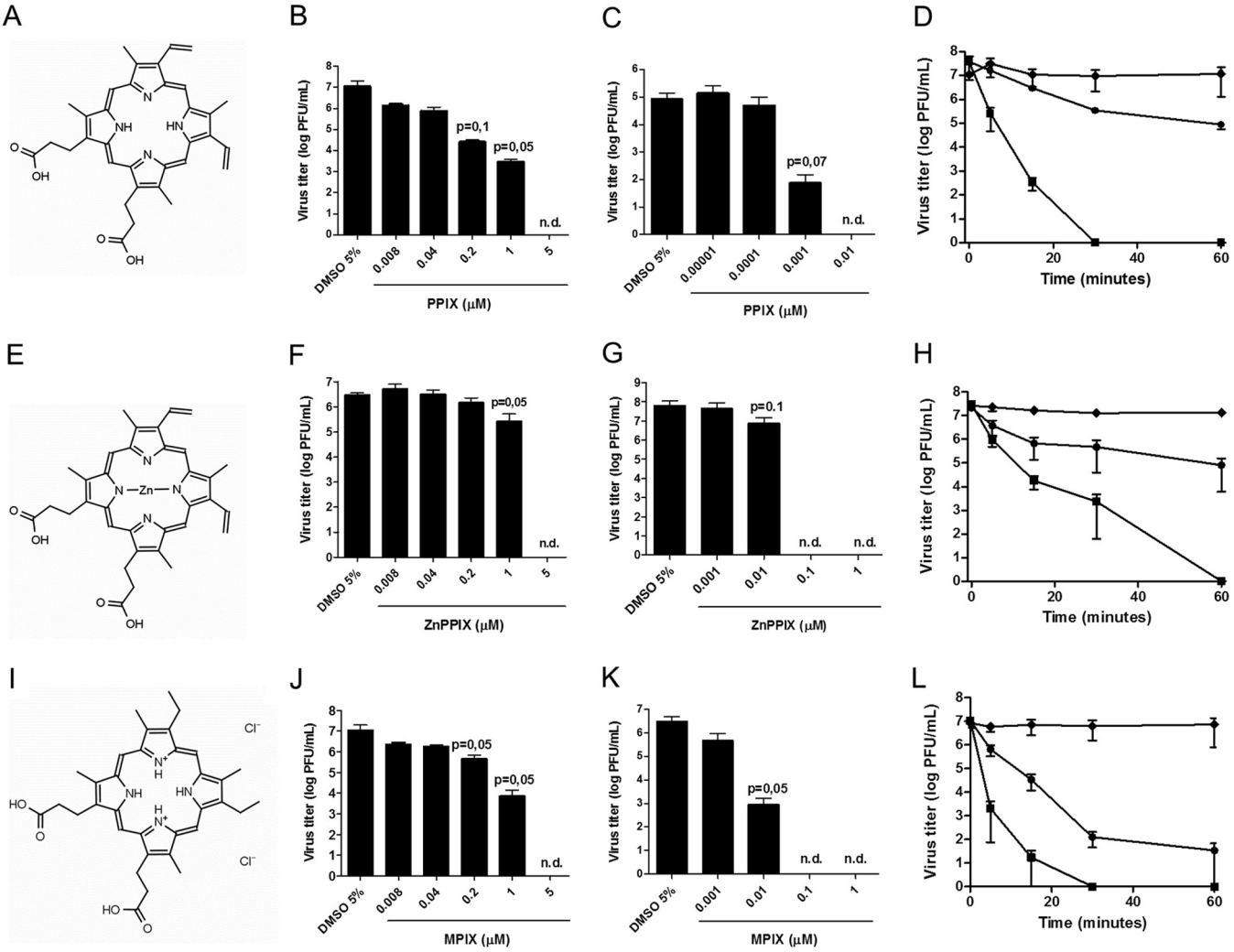

FIG 1 PPIX (A to D), ZnPPIX (E to H), and MPIX (I to L) inactivate VSV. The molecular structures of PPIX (A), ZnPPIX (E), and MPIX (I) are shown. VSV was incubated with the indicated concentrations of the porphyrins for 1 h in the dark (B, F, and J) or under illumination using a 30-W fluorescent lamp with a luminous emittance of 2,000 lx positioned 10 cm from the sample (C, G, and K), and the virus infectivity of BHK-21 cells was assessed by plaque assay. The kinetics of VSV inactivation under photoactivating conditions was evaluated for PPIX at 0.001 μM (●) and 0.01 μM (■) concentrations (D), for ZnPPIX at 0.01 μM (●) and 0.1 μM (■) concentrations (H), and for MPIX at 0.01 μM (●) and 0.1 μM (■) concentrations (L). As controls, the titers of VSV samples incubated with 5% DMSO under the same conditions were measured (◆). Data are represented as means ± SEMs for at least three independent samples. *P* values (for porphyrin-treated versus nontreated samples) are shown on the top each bar. n.d., not determined.

RESULTS

Treatment with PPIX, ZnPPIX, and MPIX inactivates VSV. VSV was incubated with different concentrations of PPIX, ZnPPIX, and MPIX for 1 h either in the dark or under light to promote their photoactivation, and virus infectivity was evaluated by plaque assay (Fig. 1). All porphyrins tested presented anti-VSV activity even without photoactivation, with the reduction in viral titer being about 10-fold for ZnPPIX and 1,000-fold for PPIX and MPIX when they were each used at a 1 μM concentration. At 5 μM, all porphyrins tested were able to completely abolish VSV infectivity (Fig. 1B, F, and J). To precisely compare the antiviral activity of each porphyrin, the half-maximal (50%) inhibitory concentrations (IC_{50}s) were calculated (Table 1).

Photoactivation of the porphyrins significantly enhanced their antiviral activities, with 0.1 μM ZnPPIX, 0.01 μM PPIX, and 0.1 μM MPIX completely abolishing VSV infectivity (Fig. 1C, G, and K, respectively). The IC_{50}s of the photoactivated porphyrins against VSV were also calculated (Table 1). Photoactivated ZnPPIX and PPIX showed IC_{50}s against VSV 100-fold lower than those observed with nonphotoactivated ZnPPIX and PPIX, while the IC_{50} of photoactivated MPIX was decreased about 50-fold relative

TABLE 1 Porphyrin IC_{50}s against VSV

Porphyrin	Mean IC_{50} ± SEM (nM)	
	Nonphotoactivated	Photoactivated
PPIX	8.294 ± 1.013	0.09764 ± 0.002566
ZnPPIX	101.5 ± 34.18	1.028 ± 0.5577
MPIX	47.18 ± 26.21	0.9659 ± 0.5499

to that of nonphotoactivated MPIX. We also characterized the kinetics of porphyrin-induced VSV inactivation under photoactivating conditions, using 0.001 μM and 0.01 μM PPIX (Fig. 1D), 0.01 μM and 0.1 μM ZnPPIX (Fig. 1H), or 0.01 μM and 0.1 μM MPIX (Fig. 1L). Altogether, these data suggest that all porphyrins tested have anti-VSV activity, which is enhanced by photoactivation.

PPIX, ZnPPIX, and MPIX interact with VSV envelope. Porphyrins are amphipathic molecules that interact with biological membranes (19). PPIX, ZnPPIX, and MPIX are fluorescent porphyrins, and their fluorescence emission increases as the polarity of the medium decreases (Fig. 2A to C). Using this property, it was possible to calculate their partition coefficients (K_ps) for membranes of different lipid compositions. For this, we recorded the PPIX, ZnPPIX, and MPIX fluorescence emission spectra after progressive

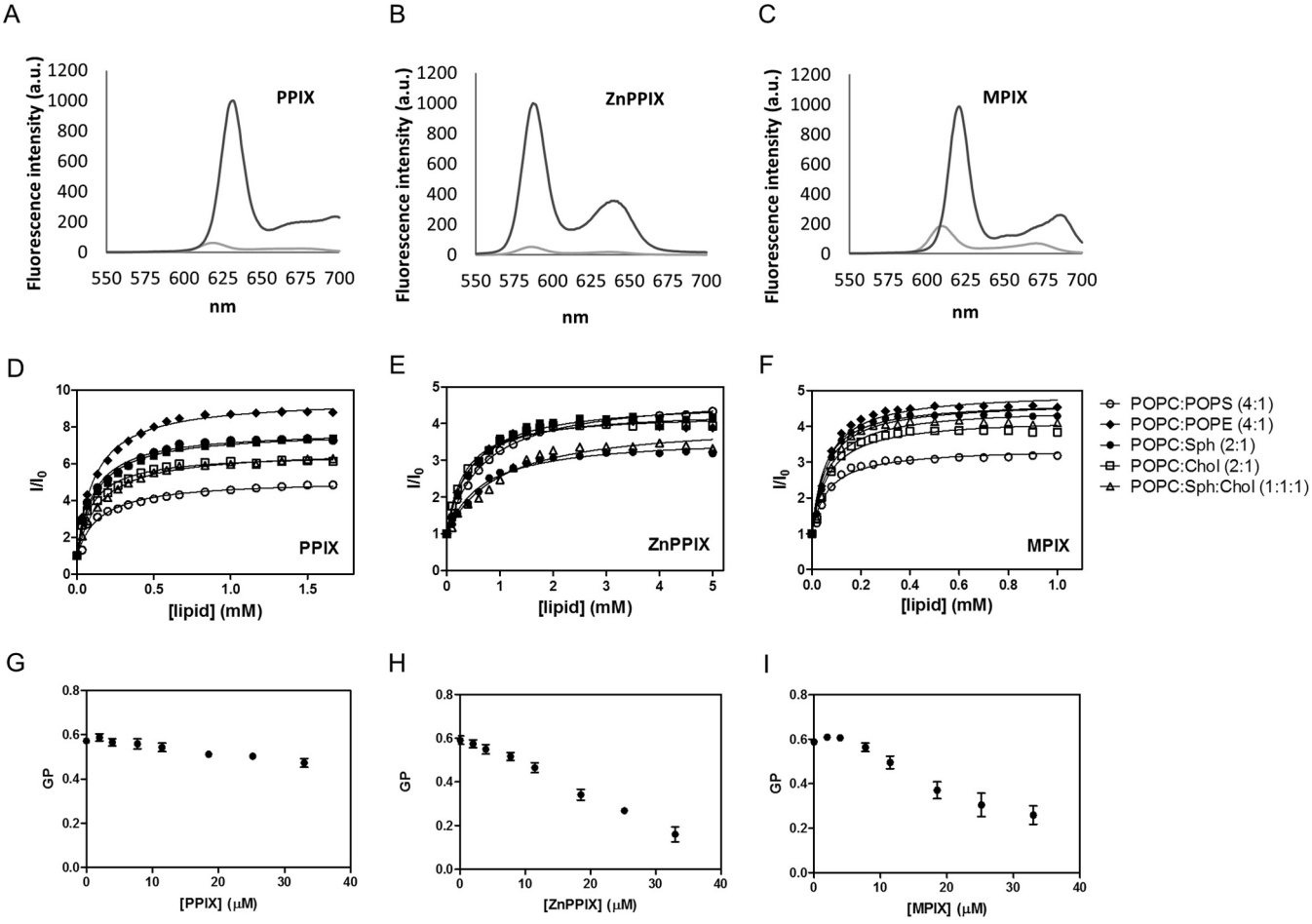

FIG 2 PPIX, ZnPPIX, and MPIX interact with lipid membranes and interfere with VSV membrane ordering. (A to C) Fluorescence emission spectra of PPIX (A), ZnPPIX (B), and MPIX (C) in PBS (light gray curves) and in ethanol (dark gray curves). Excitation wavelengths were 394, 407, and 394 nm for PPIX, ZnPPIX, and MPIX, respectively. a.u., arbitrary units. (D to F) Partition curves of PPIX (D), ZnPPIX (E), and MPIX (F) to PC (100%), PC-PE (4:1), PC-PS (4:1), PC-Chol (2:1), PC-Sph (2:1), or PC-Sph-Chol (1:1:1) vesicles obtained by progressive LUV addition to a solution of 2.8 μM for ZnPPIX and PPIX and 2.6 μM for MPIX. *I*, fluorescence intensity in the presence of LUVs; I_0, fluorescence intensity in the absence of LUVs. (G to I) Laurdan GP values after progressive addition of PPIX (G), ZnPPIX (H), and MPIX (I) to a solution containing laurdan-labeled VSV. GP values were calculated as described in Materials and Methods using the emission peaks at 440 and 490 nm. All data correspond to means ± SEMs from at least three independent experiments.

TABLE 2 Membrane K_p for PPIX, ZnPPIX, and MPIX

	Mean K_p ± SEM (10^3)		
Lipid mixture	**PPIX**	**ZnPPIX**	**MPIX**
POPC-POPS (4:1)	8.30 ± 0.99	1.63 ± 0.19	21.47 ± 1.41
POPC-POPE (4:1)	14.10 ± 0.99	2.91 ± 0.31	25.99 ± 4.35
POPC-Chol (2:1)	10.91 ± 2.854	3.62 ± 0.22	14.95 ± 2.13
POPC-Sph (2:1)	11.60 ± 0.76	2.99 ± 0.50	21.73 ± 0.09
POPC-Sph-Chol (1:1:1)	12.83 ± 2.19	1.75 ± 0.41	19.08 ± 0.71

addition of large unilamellar vehicles (LUVs) composed of 1-palmitoyl-2-oleyl-*sn*-glycero-3-phosphatidylcholine (POPC)–1-palmitoyl-2-oleyl-*sn*-glycero-3-phosphatidylethanolamine (POPE) (4:1), POPC–1-palmitoyl-2-oleyl-*sn*-glycero-3-phosphatidylserine (POPS) (4:1), POPC-cholesterol (Chol) (2:1), POPC-sphingomyelin (Sph) (2:1), and POPC-Sph-Chol (1:1:1) and plotted the spectral area as a function of the lipid concentration (Fig. 2D to F). All porphyrins tested were able to interact with LUVs with high K_p values (Table 2). No significant difference in the compositions of the different LUVs was detected, but MPIX and PPIX presented higher K_p values than ZnPPIX for all LUVs tested.

Although the porphyrins' partition to LUVs is a good tool for studying the porphyrin-membrane interaction, viral envelopes contain proteins at a high density, and these proteins may interfere with membrane disturbance by porphyrins. Thus, to evaluate the porphyrin-membrane interaction in the virus context, we used laurdan generalized polarization (GP) to assess the porphyrin-induced changes in viral envelope ordering. PPIX, ZnPPIX, and MPIX were progressively added to a solution containing VSV that had previously been labeled with laurdan, and laurdan spectral shifts were used for GP calculation. All porphyrins tested induced a laurdan GP decrease, indicating changes in the membrane ordering of the VSV envelope (Fig. 2G to I). Interestingly, photoactivated porphyrins promoted the same GP changes as those induced by nonphotoactivated porphyrins (data not shown), suggesting that porphyrin partition to the VSV envelope is not dependent on its photoactivation. This result also supports the suggestion that the laurdan spectral shifts observed in labeled VSV are due to changes in viral membrane ordering and are not yet due to the total envelope disruption promoted by the ROS generated during the porphyrin photoactivation process.

PPIX, ZnPPIX, and MPIX promote VSV G glycoprotein cross-linking. To evaluate whether PPIX, ZnPPIX, and MPIX had any effect on VSV proteins, protein damage in VSV incubated with photoactivated and nonphotoactivated porphyrins was evaluated by SDS-PAGE. The VSV protein profile in 10% SDS-polyacrylamide gels allowed the observation of 4 of the 5 viral structural proteins: the L protein (241 kDa), G glycoprotein (55 kDa), N nucleoprotein (47 kDa), and M (matrix) protein (26 kDa) (Fig. 3). Interestingly, a band of approximately 130 kDa was observed for ZnPPIX-, PPIX-, and MPIX-treated VSV samples. For the virus treated under nonphotoactivating conditions, this band became evident at a porphyrin concentration of 5 μM, while for photoactivated porphyrin-treated VSV samples, it appeared after treatment with lower porphyrin concentrations (Fig. 3). This band could correspond either to cross-linked viral proteins or to an L protein degradation product. To discriminate these possibilities, the 130-kDa band was extracted from the gel and submitted to mass spectrometry (MS) analyses. The results showed the presence of G glycoprotein, suggesting that the band corresponds to large complexes of G glycoproteins (data not shown). Additionally, for photoactivated samples, the G glycoprotein band seemed to be significantly reduced in VSV treated with MPIX at a 1 μM concentration. The M protein band was also reduced in VSV samples under this condition. Taken together, these results suggest that PPIX, ZnPPIX, and MPIX induce VSV G glycoprotein cross-linking, which is enhanced by porphyrin photoactivation. In this context, the loss of infectivity of porphyrin-treated VSV may be explained by G glycoprotein cross-linking in the virus envelope.

PPIX, ZnPPIX, and MPIX photoactivation induces $^1O_2$ generation. The enhanced loss of infectivity and the enhanced G glycoprotein cross-linking in photoactivated

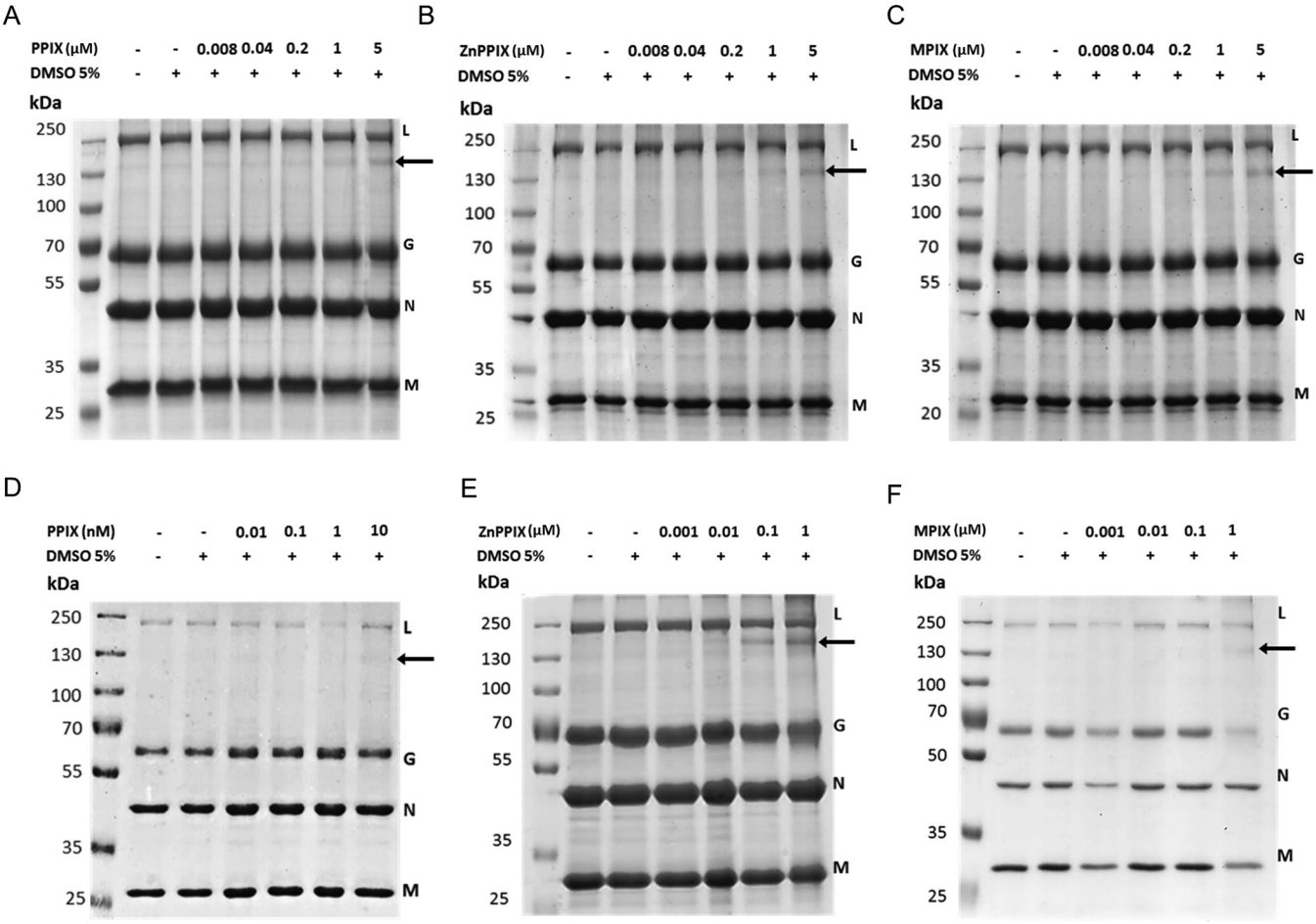

FIG 3 VSV treatment with PPIX, ZnPPIX, and MPIX promotes G glycoprotein cross-linking. VSV was incubated with the indicated concentrations of PPIX, ZnPPIX, and MPIX for 1 h in the dark (A to C) or under illumination, provided using a 30-W fluorescent lamp with a luminous emittance of 2,000 lx positioned 10 cm from the sample (D to F), and the VSV protein profile was assessed by 10% SDS-PAGE. Arrows, the band corresponding to G protein cross-linking. Images are representative of those from three independent experiments.

porphyrin-treated VSV suggest that ROS generation may be implicated in porphyrin antiviral activity. To test which reactive oxygen species is generated by PPIX, ZnPPIX, and MPIX photoactivation, porphyrin-treated VSV samples were incubated with different antioxidants and VSV infectivity was measured. Treatment with reduced glutathione, a free radical scavenger with a type I mechanism, did not alter photoactivated porphyrin-induced VSV inactivation at all concentrations tested (Fig. 4A to C). On the other hand, the loss of infectivity observed for PPIX-, ZnPPIX-, or MPIX-treated VSV under photoactivating conditions was partially reversed by treatment with sodium azide (Fig. 4D to F) and α-tocopherol (Fig. 4G to I), water- and lipid-soluble $^1O_2$ quenchers (type II mechanism), respectively. These results suggest that $^1O_2$ may be the primary ROS produced by photoactivation of these porphyrins when they are in contact with the VSV envelope. Interestingly, α-tocopherol, a lipid-soluble $^1O_2$ quencher, was more effective in protecting MIPX-treated VSV (Fig. 4I).

Altogether, these results suggest that $^1O_2$ generation in the VSV envelope by photoactivated porphyrins promotes G glycoprotein cross-linking and, consequently, viral inactivation. To obtain further evidence to confirm this hypothesis, we evaluated the ability of photoactivated PPIX, ZnPPIX, and MPIX to generate $^1O_2$, using for this 9,10-dimethylanthracene (DMA), a $^1O_2$-specific trap. Although DMA oxidation by $^1O_2$ can be observed by fluorescence quenching, the absorbance of the porphyrins near the DMA excitation wavelength impaired its use here in fluorescence experiments for $^1O_2$ detection. For this reason, DMA conversion by porphyrin-originated $^1O_2$ was evaluated

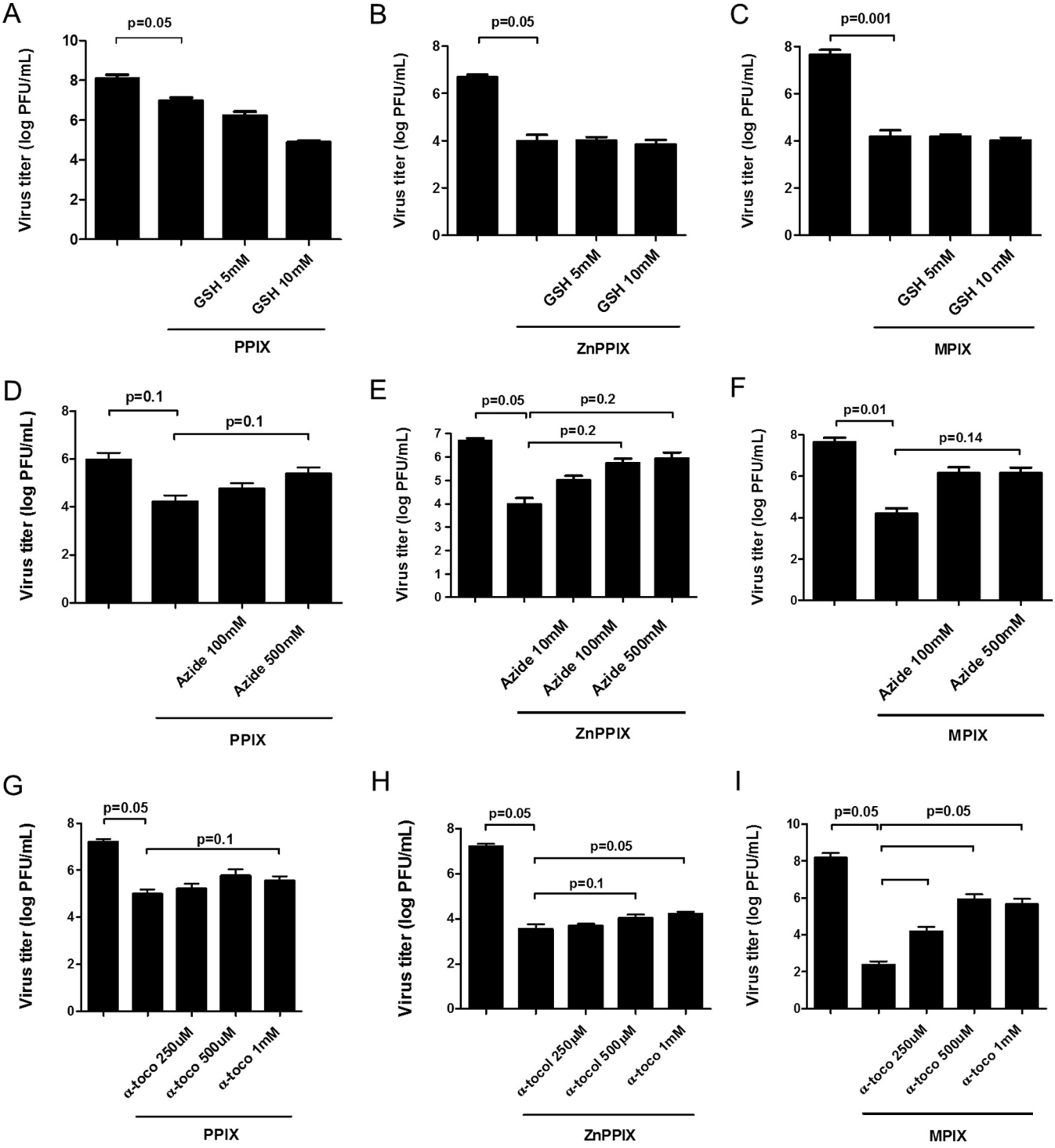

FIG 4 $^1O_2$ quenchers protect VSV from photoactivated PPIX, ZnPPIX, and MPIX antiviral activity. VSV particles were treated with 0.01 μM PPIX (A, D, and G), 0.1 μM ZnPPIX (B, E, and H), or 0.1 μM MPIX (C, F, and I) and simultaneously incubated with glutathione (GSH) (A to C), sodium azide (D to F), and α-tocopherol (α-toco) (G to I) at the indicated concentrations for 5 min under photoactivating conditions. Virus infectivity was assessed by plaque assay in BHK-21 cells. Data are represented as means $\pm$ SEM for at least three independent samples. *P* values are indicated.

by ^{1}H nuclear magnetic resonance (NMR), taking advantage of the fact that the DMA and oxidized DMA (oxi-DMA) methyl peaks could be easily identified at 3.1 ppm and 2.1 ppm, respectively (Fig. 5A). The time-dependent $^1O_2$ generation by photoactivated porphyrins is shown in Fig. 5B to D. After 30 min of incubation with 0.001 μM PPIX, 0.1 μM ZnPPIX, or 0.01 μM MPIX, all DMA was converted to oxi-DMA. This result confirms

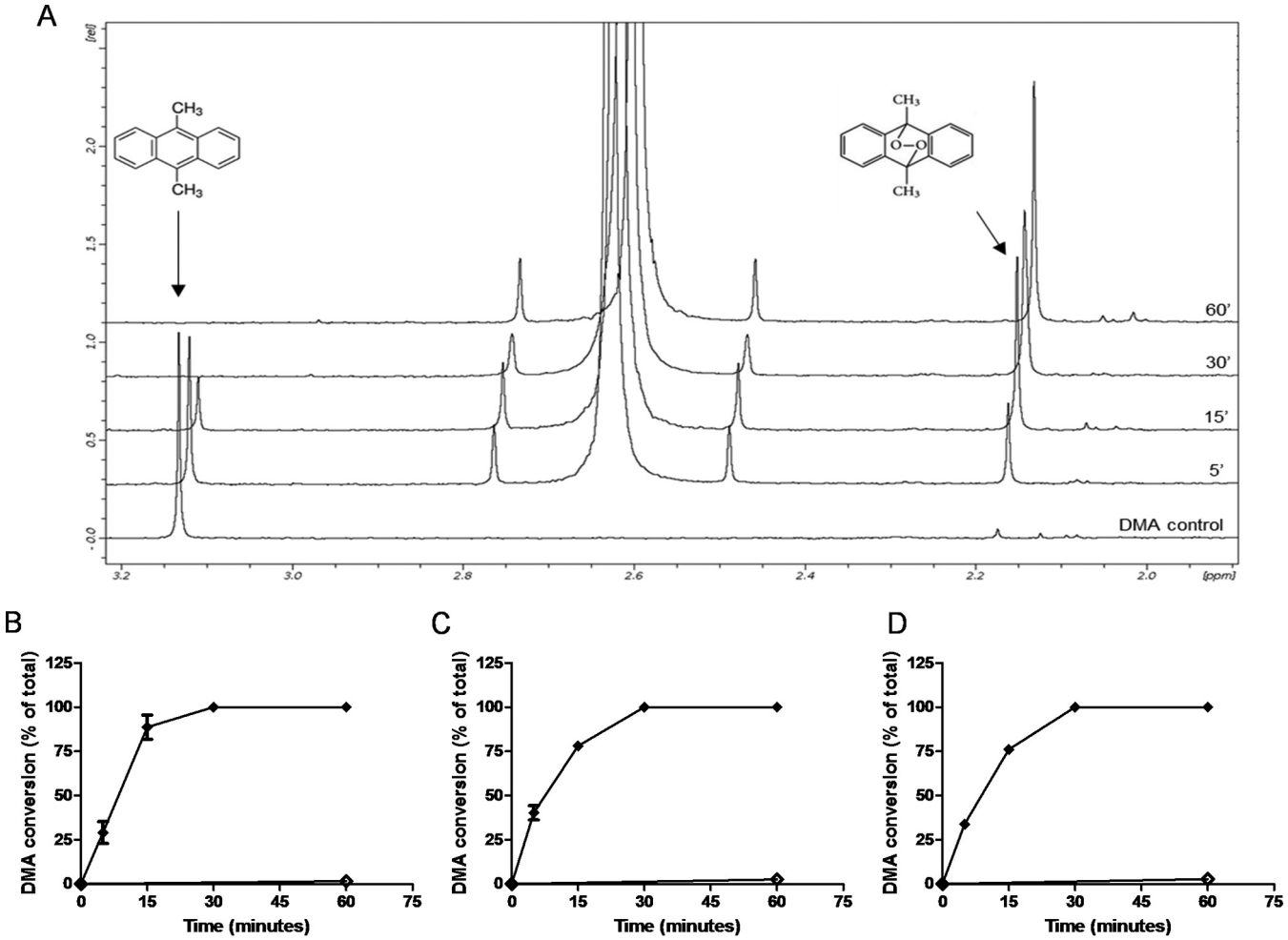

FIG 5 $^1O_2$ formation by photoactivation of porphyrins. (A) DMA/oxi-DMA conversion was evaluated by ^{1}H NMR, comparing the DMA methyl peaks at 3.1 ppm and 2.1 ppm, respectively. PPIX (B), ZnPPIX (C), and MPIX (D) at final concentrations of 0.001 μM, 0.1 μM, and 0.01 μM, respectively, were added to a solution of 20 μM DMA in chloroform and exposed to visible light (provided by a 30-W lamp with luminous emittance of 2,000 lx at a distance of 10 cm) (◆). As controls, the spectra of nonphotoactivated samples (◇) were recorded after 60 min of incubation in the dark. The data represent the means of two independent measurements. rel, relative peak intensity.

that $^1O_2$ is the main ROS produced by photoactivation of PPIX, ZnPPIX, and MPIX (type II mechanism) and is probably responsible for viral protein damage.

Porphyrins inactivate VSV during cell infection without a loss of cellular viability. To evaluate the potential application of porphyrin-induced viral inactivation to disease treatment or blood disinfection, we performed a set of experiments in which the infection assay was carried out with the virus and the porphyrins added to the cell culture at the same time (Fig. 6A). We found that even using this alternative experimental design, VSV inactivation could be observed, although to a lesser extent than when the purified virus was previously incubated with the porphyrins. It is important to highlight that even at concentrations that induced viral titer decrease, cell viability was preserved (Fig. 6B), reinforcing the potential clinical use of PPIX, ZnPPIX, and MPIX as antivirals.

DISCUSSION

Viral envelopes are promising targets for broad-spectrum antiviral agents, since the membranes of all enveloped viruses are relatively similar, as they derive from the host cell membrane. Envelope-targeted antivirals would act by affecting lipid bilayer fluidity, impairing the fusion between viral and cellular membranes, an essential event for a successful viral infection (34, 35). In this context, porphyrins appear to be good candidates for broad-spectrum antiviral agents, as they can induce membrane disorder and permeability, even independently of photoactivation-induced ROS generation (19).

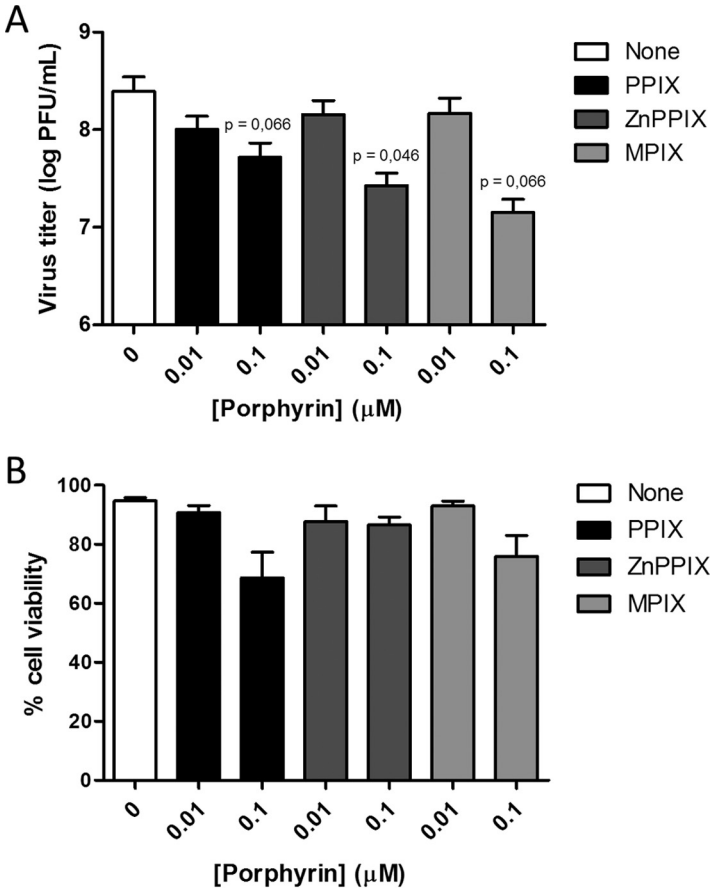

FIG 6 VSV is inactivated by PPIX, ZnPPIX, and MPIX treatment during cell infection. (A) Viral inactivation by porphyrins was performed during cell infection with VSV. BHK-21 cells were infected with an MOI of 1, concomitantly with treatment with porphyrins at the indicated concentrations, for 1 hour, under illumination using a 30-W fluorescent lamp of luminous emittance of 2,000 lx, positioned 10 cm from the sample. After 6 h, culture media were collected and frozen. Virus titers were quantified by plaque assay in BHK-21 cells. (B) Porphyrin cytotoxicity was assessed in BHK-21 cells. Cells were incubated with different concentrations of PPIX, ZnPPIX, and MPIX in culture medium without FBS for 1 hour, under illumination using a 30-W fluorescent lamp of luminous emittance of 2,000 lx, positioned 10 cm from the sample. Then, cell viability was evaluated using the MUSE count and viability kit (Millipore). Data are represented as means ± SEM from at least three independent samples. *P* values are indicated in the figure.

In this work, we analyzed the inactivation of the enveloped virus VSV by three porphyrins, PPIX, MPIX, and ZnPPIX. In addition to its economic and veterinary importance, VSV is a good model for viral inactivation studies since it is a fast-growing and easily titrated virus. Incubation of VSV with the three porphyrins tested decreased its infectivity in a concentration-dependent manner. The antiviral action of PPIX, MPIX, and ZnPPIX without photoactivation may be attributed to their ability to intercalate membranes, as demonstrated by studies of their partition into LUVs. MPIX and PPIX presented higher K_p values than ZnPPIX, as expected because of their high hydrophobicities. Accordingly, the interaction between porphyrins and membranes seems to be dependent only on hydrophobicity, since no significant difference in the porphyrin-LUV interaction was observed for vesicles of different lipid compositions. In addition, all three porphyrins interfered with viral membrane ordering, leading to a decrease in laurdan GP values, although no membrane phase transition was observed. These results confirm the porphyrin interaction with the VSV envelope and may be correlated with VSV inactivation. Furthermore, PPIX and MPIX, which show a higher affinity to membranes than ZnPPIX, were slightly more effective than ZnPPIX in inactivating VSV, corroborating the hypothesis that virus inactivation depends on porphyrin insertion into the viral envelope.

Porphyrins not only are hydrophobic molecules, but they also show a photoactive character, two features that make them attractive for PDT against enveloped viruses. Indeed, the majority of the photosensitizers used in PDT against microorganisms are based on the backbone of tetrapyrroles (2, 20). Accordingly, here we showed that the antiviral activity of PPIX, MPIX, and ZnPPIX against VSV was significantly potentiated by photoactivation, suggesting that inactivation efficiency would depend on the generation of deleterious ROS by porphyrin photoactivation close to envelope lipids and proteins, irreversibly reacting with them. In agreement with this idea, our results demonstrated that MPIX, followed by PPIX, had a greater affinity for membrane lipids as MPIX and PPIX presented higher K_p values in the partition experiments, together with higher antiviral activity, than ZnPPIX. Surprisingly, the antiviral activity of photoactivated ZnPPIX was comparable to that of photoactivated MPIX, suggesting that the antiviral activity of ZnPPIX may reside more in its ability to generate ROS when it is photoactivated than in its hydrophobic character.

The appearance of a G protein-containing band of approximately 130 kDa in the electrophoretic analysis of viral proteins after treatment with porphyrins, together with a decrease in the intensity of the typical G protein band, suggests that G protein cross-linking occurs in porphyrin-treated VSV. Although cross-linking was also observed in nonphotoactivated porphyrin-treated VSV (when porphyrin was used at higher concentrations), these results imply that ROS generation by photoactivated porphyrins promotes G protein damage, which is involved in virus inactivation. In this regard, the relatively high rate constants for the $^1O_2$ reaction with some protein side chains make the proteins the main target for photodynamic agents (36, 37), and both cross-linking between proteins and protein degradation can be a result of the oxidation mediated by the photosensitizer (37, 38). The G protein damage induced by photoactivated MPIX was more evident than that caused by ZnPPIX. In addition, a decrease in the M protein band intensity was also observed for VSV samples treated with photoactivated MPIX, corroborating the hypothesis that this porphyrin inserts deeper into the VSV envelope than the others. Porphyrin derivatives and phthalocyanines were also shown to have photodynamic antiviral activity against VSV (24, 25, 39–42), but although protein cross-linking was reported in one of these studies (39), the mechanisms by which protein damage was caused by the photoactivated molecule was not well documented.

We used three different antioxidants to determine which ROS generation pathway was involved in PPIX, ZnPPIX, and MPIX antiviral activity. We found that sodium azide and α-tocopherol partially protected VSV from inactivation by the porphyrins, showing that $^1O_2$ is the deleterious species involved in the antiviral activity of the photoactivated porphyrins. The detection of the oxi-DMA methyl peak in the NMR spectrum of photoactivated porphyrin reinforced this hypothesis. Interestingly, α-tocopherol was more effective than sodium azide in protecting VSV from the antiviral activity of MPIX. These results agree with the hypothesis that MPIX, being more hydrophobic, would act deeper in the virus envelope, so that a hydrophobic $^1O_2$ quencher, like α-tocopherol, would be more effective than a soluble one, like sodium azide.

For a long time, PDT research was mostly targeted to cancer therapy, leading to the approval of manifold PDT protocols for the treatment of malignant and nonmalignant conditions (20, 43), with many porphyrin-related molecules being submitted to clinical trials and clinical approval being obtained for some of them (20). For instance, the PPIX precursor, 5-aminolevulinic acid (ALA), has been successfully used in the topical treatment of skin cancer and other dermatologic lesions (20, 44, 45). On the other hand, although PDT was first proposed as a means to kill microorganisms, only with the emergence of multidrug-resistant microorganisms has the use of PDT against microbes been revisited (20, 46). Since then, several attempts to discover photosensitizing drugs suitable for antimicrobial and antiviral therapies have been made. As examples, viral lesions were cleared both by ALA-PDT treatment of herpes simplex virus-infected animals and through light irradiation of cell-accumulated PPIX in an HIV-infected patient (47). Here we provide preliminary data demonstrating that noncytotoxic doses

of porphyrins present antiviral activity directly on cultured cells. In this context, topical antiviral treatment with these porphyrins should be further investigated.

Finally, regardless of the significant reduction of pathogen transmission by blood and derivatives through pathogen screening and donor counseling, the risk, involving the window period of contamination, still persists (48, 49). In order to minimize this risk, the development of new approaches of blood disinfection with drugs targeting a broad range of pathogens should be addressed. The use of porphyrins and its analogs in PDT for viral inactivation of blood products has proved successful (24, 25, 28, 50, 51), and VSV is often used as a model virus in such tests (24, 25, 41). In this context, PPIX, ZnPPIX, and MPIX could be used for blood disinfection as well and should be tested for their cytotoxicity for blood cells.

In conclusion, although the findings of other studies on the use of porphyrins in PDT against several viruses are available, in this work we not only show by different and complementary techniques that PPIX, ZnPPIX, and MPIX have antiviral activity against VSV but also describe the mechanism involved in these processes, which includes porphyrin intercalation into the virus envelope lipid bilayer with changes in lipid ordering and $^1O_2$ production after their photoactivation.

MATERIALS AND METHODS

Materials and sample preparation. PPIX, ZnPPIX, and MPIX were purchased from Frontier Scientific. All porphyrins were diluted in dimethyl sulfoxide (DMSO) to a stock concentration of 50 mM and frozen at −20°C. All solutions were prepared in the dark. For the experimental procedures, porphyrins were diluted in culture medium, with the final DMSO concentration being maintained at 5%, which did not affect VSV infectivity (data not shown). 1-Palmitoyl-2-oleyl-*sn*-glycero-3-phosphatidylcholine (POPC), 1-palmitoyl-2-oleyl-*sn*-glycero-3-phosphatidylserine (POPS), 1-palmitoyl-2-oleyl-*sn*-glycero-3-phosphatidylethanolamine (POPE), sphingomyelin (egg), and cholesterol were purchased from Avanti Polar Lipids. Large unilamellar vesicles (LUVs) with an average diameter of 100 nm were prepared by extrusion methods as described previously (52, 53). 2-Dimethylamino-6-lauroylnaphthalene (laurdan) and 9,10-dimethylanthracene (DMA) were obtained from Sigma-Aldrich. α-Tocopherol and glutathione (GSH) were purchased from Sigma-Aldrich. Sodium azide was acquired from USB Corporation. GSH and sodium azide stock solutions (250 mM and 1 M, respectively) were prepared in Milli-Q water, while the 200 mM α-tocopherol stock solution was prepared in ethanol. For virus incubation, α-tocopherol was first diluted to 50 mM in ethanol and then diluted in culture medium to 1 mM and 500 μM (2% and 1% ethanol, respectively). The final ethanol concentrations used did not alter the VSV titer (data not shown).

Cell culture. BHK-21 cells were cultured in alpha minimum essential medium (α-MEM; Gibco, Life Technologies Inc.) supplemented with 10% fetal bovine serum (FBS; LGC Biotecnologia) at 37°C in a 5% CO_2 atmosphere.

Virus propagation and purification. The VSV Indiana strain was propagated in BHK-21 cells. Cells were infected at a multiplicity of infection (MOI) of 0.1, and after 16 to 20 h, the conditioned medium containing the virus particles was harvested and centrifuged at 2,000 × *g* for 30 min to remove the cell debris. The supernatant was centrifuged at 36,000 rpm for 2 h 30 min at 4°C using a Beckman Ti45 rotor. Afterward the supernatant was discarded and the pellet containing the VSV particles was incubated with 3E buffer (120 mM Tris, 60 mM sodium acetate, 3 mM EDTA, pH 7.4) at 4°C overnight. Then, the pellet was resuspended and deposited in a discontinuous gradient of 15% and 60% (wt/vol) sucrose in 3E buffer and centrifuged at 36,000 rpm for 1 h at 4°C using a Beckman SW-41 rotor. The visible virus band was collected, and the buffer was changed to phosphate-buffered saline (PBS; pH 7.4) using an Amicon 3K system (Merck, Millipore Ltd.). Purification was confirmed by SDS-PAGE. The virus titer and protein concentration were determined by plaque assay in BHK-21 cells and the Lowry method, respectively. Purified virions were stored at −70°C.

Virus titration by plaque assay. The virus titer was quantified by plaque assay in BHK-21 cells. Virus samples were serially diluted in α-MEM, and after 1 h of infection, 1% carboxymethyl cellulose in α-MEM with 2% (vol/vol) FBS was added to the wells. Cells were kept in culture at 37°C in a 5% CO_2 atmosphere for 16 h. The cells were then fixed with 4% formaldehyde solution and stained with crystal violet (1% [wt/vol] crystal violet powder in 20% methanol) for plaque visualization.

Porphyrin treatment for VSV inactivation. Purified VSV particles were incubated for 1 h in the dark with different concentrations of PPIX, ZnPPIX, and MPIX in culture medium without FBS. For determination of the antiviral activity of the photoactivated porphyrins, treated VSV particles were illuminated using a 30-W fluorescent lamp with a luminous emittance of 2,000 lx positioned 10 cm from the sample. The half-maximal (50%) inhibitory concentration (IC_{50}) was determined by nonlinear regression with a sigmoidal and variable slope profile using GraphPad Prism (version 6.0) software. To evaluate the antiviral activities of the porphyrins when they were added directly to the cell culture, VSV infection was carried out with nonpurified virus at an MOI of 1, different concentrations of PPIX, ZnPPIX, and MPIX were immediately added to culture medium without FBS, and the culture was incubated at room temperature for 1 h under illumination as described above. After 1 h of infection, the culture medium was replaced with medium supplemented with 10% FBS. At 6 h postinfection (hpi), conditioned medium was collected and the virus titer was determined by plaque assay.

Cell viability assays. BHK-21 cells were incubated for 1 h under illumination as described above with different concentrations of PPIX, ZnPPIX, and MPIX in culture medium without FBS. Then, cell viability was evaluated using a Muse count and viability kit (Millipore) as described by the manufacturer.

Antioxidant treatment. Prior to VSV treatment with porphyrins, GSH, sodium azide, or α-tocopherol was added to the viral samples, followed immediately by incubation with the porphyrins for 5 min under illumination with a 30-W fluorescent lamp with a luminous emittance of 2,000 lx positioned 10 cm from the sample. After incubation, the virus suspensions were diluted at least 10-fold in culture medium for titration.

Analysis of viral proteins after porphyrin treatment. Proteins from control or porphyrin-treated VSV were analyzed by 10% SDS-PAGE followed by Coomassie blue G staining. The modified viral proteins were identified by nano-liquid chromatography (LC)- tandem mass spectrometry (MS/MS) after in-gel digestion (data not shown). The sections of interest were manually excised and submitted to trypsin digestion. To remove the stain, the sections were washed by incubation overnight with 25 mM NH_4HCO_3 in 50% acetonitrile at room temperature. The reduction of protein disulfide bonds was performed by the addition of 10 mM dithiothreitol (USB Corporation) in 25 mM NH_4HCO_3 at 56°C for 1 h, followed by a washing step with 25 mM NH_4HCO_3. The alkylation of the free SH groups was performed in the dark by the addition of 55 mM iodoacetamide in 25 mM NH_4HCO_3 (USB Corporation) for 45 min at room temperature. Gel slices were dehydrated with 100% acetonitrile and rehydrated in 10 μl of trypsin (modified sequencing grade; Promega) solution (0.01 μg μl^{-1} in 25 mM NH_4HCO_3). The digestion step occurred overnight at 37°C, and the peptides generated were extracted from the gel pieces after 2 steps of sonication for 15 min with 5% trifluoroacetic acid (TFA) dissolved in 50% acetonitrile. This solution was transferred to a clean 500-μl microtube and concentrated in a Speed-Vac system. Each sample was then solubilized in 20 μl 0.1% formic acid and 3% acetonitrile in deionized water. The extracted peptides were loaded in a nanoAcquity system (Waters) and desalted on-line using a Waters Symmetry C_{18} trap column (180 μm by 20 mm, 5 μm). The sample injection volume was typically 7.5 μl, and LC was performed by using a BEH 130 C_{18} column (100 μm by 100 mm, 1.7 μm) and eluting with a 0.5-μl/min flow with a linear gradient (10 to 40%) of acetonitrile containing 0.1% formic acid. Electrospray tandem mass spectra were recorded using a quadrupole/orthogonal acceleration time of flight (Q-Tof) spectrometer (Waters) interfaced to the nanoAcquity system capillary chromatograph. The electrospray ionization voltage was set at 3,500 V, the source temperature was 80°C, and the cone voltage was 30 V. Instrument control and data acquisition were conducted by a MassLynx data system (version 4.1; Waters), and experiments were performed by scanning at a mass-to-charge ratio (*m/z*) of from 400 to 2,000 using a scan time of 1 s, applied during the whole chromatographic process. The mass spectra corresponding to each signal from the total ion current (TIC) chromatogram were averaged, allowing for accurate molecular mass measurement. The exact mass was determined automatically using the LockSpray reference ion of the Q-Tof spectrometer (Waters). Data-dependent MS/MS acquisitions were performed on precursors with charge states of 2, 3, or 4 over a range of from 50 to 2,000 *m/z* and under a 2-*m/z* window. A maximum of three ions were selected for MS/MS from a single MS survey. Collision-induced dissociation (CID) MS/MS spectra were obtained using argon as the collision gas at a pressure of 40 lb/in^2, and the collision voltage was varied between 18 and 90 V, depending on the mass and charge of the precursor. All data were processed using a ProteinLynx Global server (version 2.5; Waters). The processing corrected automatically the *m/z* scale of both the MS and MS/MS data utilizing the LockSpray reference ion. Proteins were identified by correlation of tandem mass spectra and the NCBInr database of proteins (which contains 3,782,683 sequences in the virus database; last update, 16 November 2016) using MASCOT software (version 2.3; Matrix Science). One missed cleavage per peptide was allowed, and an initial mass tolerance of 0.1 Da was used in all searches. Cysteines were assumed to be carbamidomethylated, and variable modifications of methionine (oxidation) were allowed. An identification was considered positive if it matched at least two peptides with a mass accuracy of better than 0.1 Da.

Partition coefficient determination. Studies on porphyrin partition to membranes were performed in a Varian Cary Eclipse fluorescence spectrometer. The assay is based on the fact that the PPIX, ZnPPIX, and MPIX fluorescence emission spectra are modified by changes in medium polarity, allowing the porphyrin-membrane interaction to be quantified. The excitation wavelengths used were 394, 407, and 394 nm for PPIX, ZnPPIX, and MPIX, respectively, with the emission spectra being recorded from 550 to 700 nm. The bandwidths used were 10 nm for excitation and 5 nm for emission. Each emission spectrum was corrected for dilution and for simultaneous light absorbance by porphyrin. The experiments consisted of the successive addition of LUVs (POPC-POPE at a molar ratio of 4:1, POPC-POPS at 4:1, POPC-Chol at 2:1, POPC-Sph at 2:1, or PC-Sph-Chol at 1:1:1) to the porphyrins diluted in PBS to a concentration of 2.8 μM for ZnPPIX and PPIX and 2.6 μM for MPIX, with a 10-min incubation time being used between each addition. Calculation of the partition coefficients (K_ps) was performed as described by Santos et al. (54). The experimental data were fit using equation 1:

$$\frac{I}{I_0} = \frac{1 + K_p \cdot \gamma_L \cdot \frac{I_L}{I_0} \cdot [L]}{1 + K_p \cdot \gamma_L \cdot [L]} \quad (1)$$

where K_p is the partition coefficient; I, I_L, and I_0 are the fluorescence intensities (spectral area between 550 and 700 nm) in the presence of LUVs, in lipid environment, and in the absence of LUVs, respectively; γ_L is the lipid molar volume (we used an approximation for this value on the basis of the POPC lipid molar ratio); and [*L*] is the lipid concentration. All measurements were done at 28°C.

GP. Alteration of membrane ordering due to the porphyrin interaction was evaluated by determination of the laurdan fluorescence spectral shift, as laurdan is sensitive to polarity changes in the

medium. Viral samples at a protein concentration of 100 μg/ml were incubated with 20 μM laurdan in PBS, pH 7.4, for 20 min at 4°C. After successive porphyrin addition (with a 10-min incubation time between each addition), samples were excited at 360 nm and the fluorescence emission spectra were recorded from 400 to 600 nm using a Spectroflourimeter PC1 (ISS Inc., Champaign, IL). Laurdan generalized polarization (GP), which represents the shift in the laurdan spectrum induced by medium polarity changes, was calculated as described in equation 2, adapted from the work of Parasassi et al. (55):

$$\mathrm{GP} = \frac{I_{440} - I_{490}}{I_{440} + I_{490}} \quad (2)$$

where I_{440} and I_{490} are the emission intensities at 440 and 490 nm, respectively. All measurements were done at 28°C.

$^1O_2$ production by porphyrins. $^1O_2$ production was measured by determining DMA/oxi-DMA by NMR spectroscopy. The porphyrin solution (0.001 μM PPIX, 0.1 μM ZnPPIX, or 0.01 μM MPIX) was incubated with 20 μM DMA in NMR tubes, and the tubes were exposed or not exposed to visible light (provided by a 30-W light lamp with a luminous emittance of 2,000 lx at a distance of 10 cm) for 5, 15, 30, or 60 min. The conversion of DMA (DMA methyl peak at 3.1 ppm) to oxi-DMA (oxi-DMA methyl peak at 2.1 ppm) was measured by ^{1}H NMR. All the spectra were recorded in a 500-MHz Bruker Avance spectrometer at 298 K in deuterated $CDCl_3$. The percentages of conversion were calculated by considering the integrals of the methyl peaks in two independent measurements.

Statistical analyses. Statistical analyses were performed using GraphPad Prism (version 6.0) software. Group differences were compared using Student's *t* test.

ACKNOWLEDGMENTS

This work was supported by the Fundação Carlos Chagas Filho de Amparo à Pesquisa do Estado do Rio de Janeiro (FAPERJ; Brazil; grant number E-26/201.167/2014), the Conselho Nacional de Desenvolvimento Científico e Tecnológico (CNPq; Brazil; grant number 306669/2013-7), the Coordenação de Aperfeiçoamento de Pessoal de Nível Superior (CAPES; Brazil; grant number CsF 171/2012), the Fundação para a Ciência e Tecnologia-Ministério da Educação e Ciência (FCT-MEC; Portugal; project HIVERA/0002/2013), and Marie Skłodowska-Curie Actions (MSCA; European Commission project INPACT 644167). C.C.-O. acknowledges a Science without Borders postdoctoral fellowship from CAPES (171/2012), and J.M.F. acknowledges an FCT-MEC Ph.D. fellowship (SFRH/BD/70423/2010).

We declare that we have no conflict of interest.

REFERENCES

1. Auwarter W, Ecija D, Klappenberger F, Barth JV. 2015. Porphyrins at interfaces. Nat Chem 7:105–120. https://doi.org/10.1038/nchem.2159.
2. Costa L, Faustino MA, Neves MG, Cunha A, Almeida A. 2012. Photodynamic inactivation of mammalian viruses and bacteriophages. Viruses 4:1034–1074. https://doi.org/10.3390/v4071034.
3. Vzorov AN, Dixon DW, Trommel JS, Marzilli LG, Compans RW. 2002. Inactivation of human immunodeficiency virus type 1 by porphyrins. Antimicrob Agents Chemother 46:3917–3925. https://doi.org/10.1128/AAC.46.12.3917-3925.2002.
4. Dixon DW, Gill AF, Giribabu L, Vzorov AN, Alam AB, Compans RW. 2005. Sulfonated naphthyl porphyrins as agents against HIV-1. J Inorg Biochem 99:813–821. https://doi.org/10.1016/j.jinorgbio.2004.12.013.
5. Chen-Collins AR, Dixon DW, Vzorov AN, Marzilli LG, Compans RW. 2003. Prevention of poxvirus infection by tetrapyrroles. BMC Infect Dis 3:9. https://doi.org/10.1186/1471-2334-3-9.
6. Lin L, Hu J. 2008. Inhibition of hepadnavirus reverse transcriptase-epsilon RNA interaction by porphyrin compounds. J Virol 82:2305–2312. https://doi.org/10.1128/JVI.02147-07.
7. Guo H, Pan X, Mao R, Zhang X, Wang L, Lu X, Chang J, Guo JT, Passic S, Krebs FC, Wigdahl B, Warren TK, Retterer CJ, Bavari S, Xu X, Cuconati A, Block TM. 2011. Alkylated porphyrins have broad antiviral activity against hepadnaviruses, flaviviruses, filoviruses, and arenaviruses. Antimicrob Agents Chemother 55:478–486. https://doi.org/10.1128/AAC.00989-10.
8. Cheng Y, Tsou LK, Cai J, Aya T, Dutschman GE, Gullen EA, Grill SP, Chen AP, Lindenbach BD, Hamilton AD, Cheng YC. 2010. A novel class of meso-tetrakis-porphyrin derivatives exhibits potent activities against hepatitis C virus genotype 1b replicons in vitro. Antimicrob Agents Chemother 54:197–206. https://doi.org/10.1128/AAC.01206-09.
9. Benati FJ, Lauretti F, Faccin LC, Nodari B, Ferri DV, Mantovani MS, Linhares RE, Nozawa C. 2009. Effects of chlorophyllin on replication of poliovirus and bovine herpesvirus in vitro. Lett Appl Microbiol 49:791–795. https://doi.org/10.1111/j.1472-765X.2009.02744.x.
10. Assuncao-Miranda I, Cruz-Oliveira C, Neris RL, Figueiredo CM, Pereira LP, Rodrigues D, Araujo DF, Da Poian AT, Bozza MT. 2016. Inactivation of dengue and yellow fever viruses by heme, cobalt-protoporphyrin IX and tin-protoporphyrin IX. J Appl Microbiol 120:790–804. https://doi.org/10.1111/jam.13038.
11. Levere RD, Gong YF, Kappas A, Bucher DJ, Wormser GP, Abraham NG. 1991. Heme inhibits human immunodeficiency virus 1 replication in cell cultures and enhances the antiviral effect of zidovudine. Proc Natl Acad Sci U S A 88:1756–1759. https://doi.org/10.1073/pnas.88.5.1756.
12. Staudinger R, Abraham NG, Levere RD, Kappas A. 1996. Inhibition of human immunodeficiency virus-1 reverse transcriptase by heme and synthetic heme analogs. Proc Assoc Am Physicians 108:47–54.
13. Wen WH, Lin M, Su CY, Wang SY, Cheng YS, Fang JM, Wong CH. 2009. Synergistic effect of zanamivir-porphyrin conjugates on inhibition of neuraminidase and inactivation of influenza virus. J Med Chem 52:4903–4910. https://doi.org/10.1021/jm900515g.
14. Stojiljkovic I, Evavold BD, Kumar V. 2001. Antimicrobial properties of porphyrins. Expert Opin Investig Drugs 10:309–320. https://doi.org/10.1517/13543784.10.2.309.
15. Tappel AL. 1953. The mechanism of the oxidation of unsaturated fatty acids catalyzed by hematin compounds. Arch Biochem Biophys 44:378–395. https://doi.org/10.1016/0003-9861(53)90056-3.
16. Aft RL, Mueller GC. 1983. Hemin-mediated DNA strand scission. J Biol Chem 258:12069–12072.
17. Aft RL, Mueller GC. 1984. Hemin-mediated oxidative degradation of proteins. J Biol Chem 259:301–305.
18. Vincent SH, Grady RW, Shaklai N, Snider JM, Muller-Eberhard U. 1988. The influence of heme-binding proteins in heme-catalyzed oxidations.

Arch Biochem Biophys 265:539–550. https://doi.org/10.1016/0003-9861(88)90159-2.
19. Schmitt TH, Frezzatti WA, Jr, Schreier S. 1993. Hemin-induced lipid membrane disorder and increased permeability: a molecular model for the mechanism of cell lysis. Arch Biochem Biophys 307:96–103. https://doi.org/10.1006/abbi.1993.1566.
20. Abrahamse H, Hamblin MR. 2016. New photosensitizers for photodynamic therapy. Biochem J 473:347–364. https://doi.org/10.1042/BJ20150942.
21. Hamblin MR, Hasan T. 2004. Photodynamic therapy: a new antimicrobial approach to infectious disease? Photochem Photobiol Sci 3:436–450. https://doi.org/10.1039/b311900a.
22. Casteel MJ, Jayaraj K, Gold A, Ball LM, Sobsey MD. 2004. Photoinactivation of hepatitis A virus by synthetic porphyrins. Photochem Photobiol 80:294–300. https://doi.org/10.1562/2004-04-05-RA-134.1.
23. North J, Neyndorff H, Levy JG. 1993. Photosensitizers as virucidal agents. J Photochem Photobiol B 17:99–108. https://doi.org/10.1016/1011-1344(93)80002-Q.
24. Horowitz B, Williams B, Rywkin S, Prince AM, Pascual D, Geacintov N, Valinsky J. 1991. Inactivation of viruses in blood with aluminum phthalocyanine derivatives. Transfusion 31:102–108. https://doi.org/10.1046/j.1537-2995.1991.31291142938.x.
25. Rywkin S, Ben-Hur E, Malik Z, Prince AM, Li YS, Kenney ME, Oleinick NL, Horowitz B. 1994. New phthalocyanines for photodynamic virus inactivation in red blood cell concentrates. Photochem Photobiol 60:165–170. https://doi.org/10.1111/j.1751-1097.1994.tb05085.x.
26. Smetana Z, Mendelson E, Manor J, van Lier JE, Ben-Hur E, Salzberg S, Malik Z. 1994. Photodynamic inactivation of herpes viruses with phthalocyanine derivatives. J Photochem Photobiol B 22:37–43. https://doi.org/10.1016/1011-1344(93)06949-4.
27. Smetana Z, Ben-Hur E, Mendelson E, Salzberg S, Wagner P, Malik Z. 1998. Herpes simplex virus proteins are damaged following photodynamic inactivation with phthalocyanines. J Photochem Photobiol B 44:77–83. https://doi.org/10.1016/S1011-1344(98)00124-9.
28. Margolis-Nunno H, Ben-Hur E, Gottlieb P, Robinson R, Oetjen J, Horowitz B. 1996. Inactivation by phthalocyanine photosensitization of multiple forms of human immunodeficiency virus in red cell concentrates. Transfusion 36:743–750. https://doi.org/10.1046/j.1537-2995.1996.36896374381.x.
29. Schmidt-Erfurth U, Hasan T. 2000. Mechanisms of action of photodynamic therapy with verteporfin for the treatment of age-related macular degeneration. Surv Ophthalmol 45:195–214. https://doi.org/10.1016/S0039-6257(00)00158-2.
30. Mead DG, Ramberg FB, Besselsen DG, Mare CJ. 2000. Transmission of vesicular stomatitis virus from infected to noninfected black flies cofeeding on nonviremic deer mice. Science 287:485–487. https://doi.org/10.1126/science.287.5452.485.
31. Carneiro FA, Stauffer F, Lima CS, Juliano MA, Juliano L, Da Poian AT. 2003. Membrane fusion induced by vesicular stomatitis virus depends on histidine protonation. J Biol Chem 278:13789–13794. https://doi.org/10.1074/jbc.M210615200.
32. Albertini AA, Baquero E, Ferlin A, Gaudin Y. 2012. Molecular and cellular aspects of rhabdovirus entry. Viruses 4:117–139. https://doi.org/10.3390/v4010117.
33. Beilstein F, Obiang L, Raux H, Gaudin Y. 2015. Characterization of the interaction between the matrix protein of vesicular stomatitis virus and the immunoproteasome subunit LMP2. J Virol 89:11019–11029. https://doi.org/10.1128/JVI.01753-15.
34. Song JM, Seong BL. 2010. Viral membranes: an emerging antiviral target for enveloped viruses? Expert Rev Anti Infect Ther 8:635–638. https://doi.org/10.1586/eri.10.51.
35. Vigant F, Jung M, Lee B. 2010. Positive reinforcement for viruses. Chem Biol 17:1049–1051. https://doi.org/10.1016/j.chembiol.2010.10.002.
36. Benov L. 2015. Photodynamic therapy: current status and future directions. Med Princ Pract 24(Suppl 1):S14–S28. https://doi.org/10.1159/000362416.
37. Davies MJ. 2004. Reactive species formed on proteins exposed to singlet oxygen. Photochem Photobiol Sci 3:17–25. https://doi.org/10.1039/b307576c.
38. Davies MJ. 2003. Singlet oxygen-mediated damage to proteins and its consequences. Biochem Biophys Res Commun 305:761–770. https://doi.org/10.1016/S0006-291X(03)00817-9.
39. Lim DS, Ko SH, Kim SJ, Park YJ, Park JH, Lee WY. 2002. Photoinactivation of vesicular stomatitis virus by a photodynamic agent, chlorophyll derivatives from silkworm excreta. J Photochem Photobiol B 67:149–156. https://doi.org/10.1016/S1011-1344(02)00318-4.
40. Abe H, Wagner SJ. 1995. Analysis of viral DNA, protein and envelope damage after methylene blue, phthalocyanine derivative or merocyanine 540 photosensitization. Photochem Photobiol 61:402–409. https://doi.org/10.1111/j.1751-1097.1995.tb08630.x.
41. Rywkin S, Lenny L, Goldstein J, Geacintov NE, Margolis-Nunno H, Horowitz B. 1992. Importance of type I and type II mechanisms in the photodynamic inactivation of viruses in blood with aluminum phthalocyanine derivatives. Photochem Photobiol 56:463–469. https://doi.org/10.1111/j.1751-1097.1992.tb02189.x.
42. Moor AC, Wagenaars-van Gompel AE, Hermanns RC, van der Meulen J, Smit J, Wilschut J, Brand A, Dubbelman TM, VanSteveninck J. 1999. Inhibition of various steps in the replication cycle of vesicular stomatitis virus contributes to its photoinactivation by AlPcS4 or Pc4 and red light. Photochem Photobiol 69:353–359. https://doi.org/10.1562/0031-8655(1999)069<0353:IOVSIT>2.3.CO;2.
43. Huang Z. 2005. A review of progress in clinical photodynamic therapy. Technol Cancer Res Treat 4:283–293. https://doi.org/10.1177/153303460500400308.
44. Kennedy JC, Pottier RH, Pross DC. 1990. Photodynamic therapy with endogenous protoporphyrin IX: basic principles and present clinical experience. J Photochem Photobiol B 6:143–148. https://doi.org/10.1016/1011-1344(90)85083-9.
45. Kennedy JC, Marcus SL, Pottier RH. 1996. Photodynamic therapy (PDT) and photodiagnosis (PD) using endogenous photosensitization induced by 5-aminolevulinic acid (ALA): mechanisms and clinical results. J Clin Laser Med Surg 14:289–304.
46. Craig RA, McCoy CP, Gorman SP, Jones DS. 2015. Photosensitisers—the progression from photodynamic therapy to anti-infective surfaces. Expert Opin Drug Deliv 12:85–101. https://doi.org/10.1517/17425247.2015.962512.
47. Smetana Z, Malik Z, Orenstein A, Mendelson E, Ben-Hur E. 1997. Treatment of viral infections with 5-aminolevulinic acid and light. Lasers Surg Med 21:351–358. https://doi.org/10.1002/(SICI)1096-9101(1997)21:4<351::AID-LSM6>3.0.CO;2-P.
48. Moor AC, Dubbelman TM, VanSteveninck J, Brand A. 1999. Transfusion-transmitted diseases: risks, prevention and perspectives. Eur J Haematol 62:1–18.
49. Wainwright M. 2002. Pathogen inactivation in blood products. Curr Med Chem 9:127–143. https://doi.org/10.2174/0929867023371355.
50. Trannoy LL, Lagerberg JW, Dubbelman TM, Schuitmaker HJ, Brand A. 2004. Positively charged porphyrins: a new series of photosensitizers for sterilization of RBCs. Transfusion 44:1186–1196. https://doi.org/10.1111/j.1537-2995.2004.03275.x.
51. Trannoy LL, Terpstra FG, de Korte D, Lagerberg JW, Verhoeven AJ, Brand A, van Engelenburg FA. 2006. Differential sensitivities of pathogens in red cell concentrates to tri-P(4)-photoinactivation. Vox Sang 91:111–118. https://doi.org/10.1111/j.1423-0410.2006.00791.x.
52. Mayer LD, Hope MJ, Cullis PR. 1986. Vesicles of variable sizes produced by a rapid extrusion procedure. Biochim Biophys Acta 858:161–168. https://doi.org/10.1016/0005-2736(86)90302-0.
53. Szoka F, Olson F, Heath T, Vail W, Mayhew E, Papahadjopoulos D. 1980. Preparation of unilamellar liposomes of intermediate size (0.1-0.2 mumol) by a combination of reverse phase evaporation and extrusion through polycarbonate membranes. Biochim Biophys Acta 601:559–571. https://doi.org/10.1016/0005-2736(80)90558-1.
54. Santos NC, Prieto M, Castanho MA. 2003. Quantifying molecular partition into model systems of biomembranes: an emphasis on optical spectroscopic methods. Biochim Biophys Acta 1612:123–135. https://doi.org/10.1016/S0005-2736(03)00112-3.
55. Parasassi T, De Stasio G, Ravagnan G, Rusch RM, Gratton E. 1991. Quantitation of lipid phases in phospholipid vesicles by the generalized polarization of laurdan fluorescence. Biophys J 60:179–189. https://doi.org/10.1016/S0006-3495(91)82041-0.